International Journal of Engineering Applied Sciences and Technology, 2020
Vol. 5, Issue 3, ISSN No. 2455-2143, Pages 20-25
Published Online July 2020 in IJEAST (http://www.ijeast.com)

SPACE CHARGE EFFECT IN REFLECTED-ELECTRON-INCLUSIVE MULTIPACTOR PREDICTION FOR TE_{10} MODE RECTANGULAR WAVEGUIDES

Akoma Henry E.C.A., Aiyeola S. Yommy, Iliya S. Zakwoi, Soyinka Olukunle, Nzekwu Nwanze
National Space Research and Dev. Agency (NASRDA),
Nigeria

***Abstract*— Space charges influence the dynamics of free electrons present inside waveguide devices. This paper examines the effect of space charges on the multipactor discharge mechanism in the dominant transverse electric (TE_{10}) mode rectangular waveguide components by using a developed reflected-electron-inclusive multipactor prediction algorithm. The work assumes that the system of closely spaced charges is equivalent to a total charge that is continuously distributed in the form a sheet within the waveguide gap and accordingly provides an approximate model for computing the electric field induced by same charges. Simulation results suggest that the presence of space charges within a microwave device do not counter the initiation of a multipactor discharge. This observation may be attributed to the high impact energies of the multipacting electrons which despite the electrostatic repulsion forces created by the charges are able to sustain the phase-focusing mechanism.**

Keywords: **multipactor prediction, rectangular waveguides, reflected electrons, space charge effect**.

I. INTRODUCTION

Multipaction (MP) is a high frequency breakdown mechanism which occurs in vacuum environments. It is caused by high-power RF field-accelerated primary electrons. These electrons impact on the walls of microwave devices, such as TE_{10} rectangular waveguides, causing a resonant avalanche increase of secondary electrons. This avalanche increase can cause multipactor discharges which can lead to degradation in communication payload performance and possible failure of satcom payload devices. Because of this, multipactor prediction is a vital component of the design and fabrication of waveguide devices intended to operate at vacuum and high RF power conditions. In addition to possessing the capability to analyze the electromagnetic response of microwave devices, it is essential that multipactor predictors be able to determine the multipactor breakdown power levels of such structures with some level of accuracy [1], [2].

This paper is an extension of MP prediction research works in [3] and [4]. The developed MP predictor algorithm, in additional to accounting for reflected electrons, now includes space charge effects into the prediction process. The MP predictor is used here to investigate the effect of space charges on multipactor initiation in a typical TE_{10} rectangular waveguide. Space charges introduce mutual electron-electron repulsion forces which eventually results in electron density saturation which limit the electron multiplication process inside microwave devices. Previous literature on the subject have shown that, in filter networks where irises are present, the inclusion of space charge effects gave additional information on noise level, harmonics and reflected power; findings also showed a steady state criterion relating input power levels to multipactor breakdown thresholds [5], [6]. A common technique employed for model development in said literatures have been the Particle-In-Cell (PIC) codes. In contrast however, the MP algorithm used in this paper allows for a comprehensive modelling and tracking of individual electrons as against the Particle-In-Cell approach which assumes similar dynamics for *n*-number 'micro-electrons' clustered as a "super electron" [7]. Hence, excitation field computation values are more accurate as against the particle-to-grid weighing approach which is prone to interpolation errors [6].

II. THE MODEL

A. Flowchart of the MP Prediction Algorithm

The flowchart of the algorithm is shown in *Fig.* 1. Initial primary electrons are emitted from the bottom plate of the rectangular waveguide with an energy distribution of 2eV at a velocity perpendicular to the emission surface. Owing to the high frequencies involved, small enough time-steps are chosen for convergence of solution. In every time

International Journal of Engineering Applied Sciences and Technology, 2020
Vol. 5, Issue 3, ISSN No. 2455-2143, Pages 20-25
Published Online July 2020 in IJEAST (http://www.ijeast.com)

step, the electron first undergoes half acceleration due to electric field, a subsequent rotation due to the presence of magnetic field and a final half acceleration due to electric field. The electron-electron repulsion force induced by the space charge field is also computed. If the process has not reached the maximum number of specified gap crossings (number of impacts), it resumes again and tracking is continued until its next impact. After the specified number of gap crossings is met, tracking is stopped and the enhanced counter function, e_N, is computed.

$$e_N = \sum_i^N \delta_i \quad (1)$$

Parameter N is the total number of gap crossings (impacts), i is the index for each impact, and δ_i is the secondary electron yield (SEY) calculated for each impact. The enhanced counter function is a measure of the total number of electrons generated after several impacts, repeated over an interval *N*. For any electron that can make *N* times of impact, $e_N > 0$ [8]. MP is predicted for the power levels at which the $e_N > 1$.

B. The MP Prediction Algorithm

The field distribution for the TE_{10} mode rectangular waveguide was computed using equations (2) - (7):

$$r_s = \sqrt{\omega\mu_0/2\sigma_{coating}} \quad (2)$$

$$\alpha = \frac{r_s}{a^3 b\beta k\eta}(2b\pi^2 + a^3k^2) \text{ Np/m} \quad (3)$$

$$H_z(x,y,z,t) = \frac{jE_0}{\eta}\left(\frac{\lambda}{2a}\right)e^{-\alpha z}\cos\frac{\pi x}{a}\cos(\omega t - \beta z) \quad (4)$$

$$E_y(x,y,z,t) = E_0\, e^{-\alpha z}\sin\frac{\pi x}{a}\cos(\omega t - \beta z) \quad (5)$$

$$H_x(x,y,z,t) = -\frac{E_0}{Z_{TE}}e^{-\alpha z}\sin\frac{\pi x}{a}\cos(\omega t - \beta z) \quad (6)$$

$$E_x = E_z = H_y = 0 \quad (7)$$

Parameters $r_s, \sigma_{coating}, \alpha, H_x, H_z, E_y, E_0, \beta$ and a are the surface resistance of waveguide, the conductivity of the waveguide coating, the conductor attenuation constant, the magnetic field intensity in the *x*-axis, the magnetic field intensity in the *z*-axis, the electric field strength in the *y*-axis, the maximum electric field, propagation constant and the width of the waveguide respectively. Since multipaction occurs in a vacuum, the dielectric attenuation constant is assumed to have a zero value.

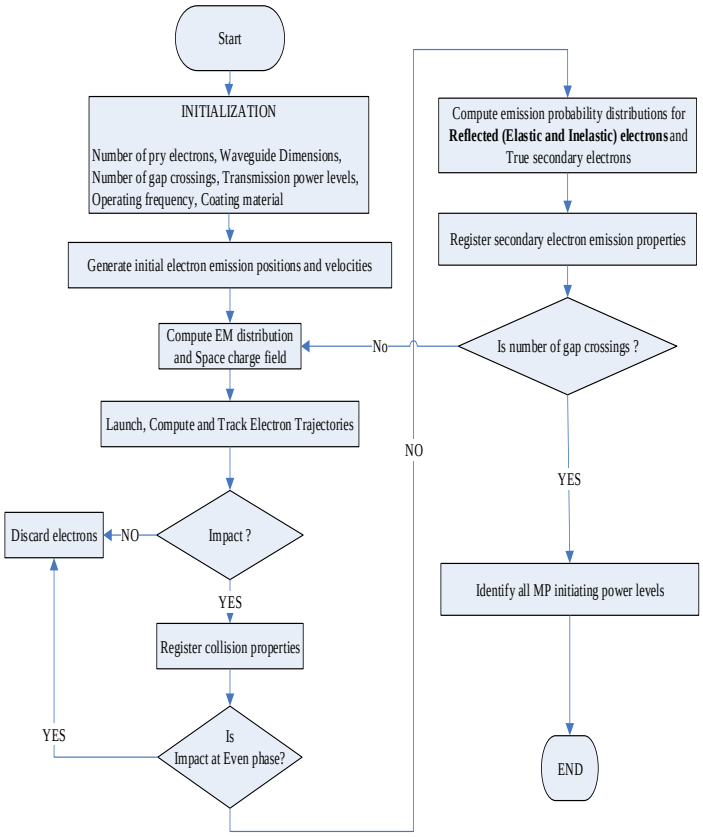

Fig. 1 MP Algorithm Flowchart

Space-charge effects can be studied with a simple hypothesis that an electron sheet is formed between metal surfaces of the waveguide components under a steady state of multipactor, as shown in *Fig. 2* [9]. The system of closely spaced charges is equivalent to a total charge that is continuously distributed along some line, over some surface, or throughout some volume [10]. Ignoring effects of fringing and discontinuity, the density of the electron sheet is given by

$$\sigma_s = -qP/A \quad (8)$$

where σ_s is the electron sheet density, P is the population size of electrons after N gap crossings, q is the electron charge and A is the surface area over which the space charges are distributed. The dynamics of each effective electron is conditioned by the EM field distribution and the repulsion of the electron sheet. Equations (9) – (11) computes the dynamics for each effective electron as they traverse the gap.

International Journal of Engineering Applied Sciences and Technology, 2020
Vol. 5, Issue 3, ISSN No. 2455-2143, Pages 20-25
Published Online July 2020 in IJEAST (http://www.ijeast.com)

$$\begin{cases} \frac{dv}{dt} = \frac{-q}{m_e}(\boldsymbol{E} + \boldsymbol{v}\,\mathrm{X}\,\boldsymbol{B} + E_{sc}) \\ \boldsymbol{v} = \frac{d\boldsymbol{R}}{dt} \end{cases} \quad (9)$$

$$E_{sc} = k_e \sigma_s w_s l_s \frac{\boldsymbol{R} - R_s}{\left|{h_s}^2 + (\boldsymbol{R} - R_s)^2\right|^{3/2}} \quad (10)$$

$$h_s = \left[\left(\frac{l_s}{2}\right)^2 + \left(\frac{w_s}{2}\right)^2\right]^{0.5} \quad (11)$$

where E_{sc} is the field produced by the space charge sheet, $\boldsymbol{R}$ is the position of an electron and R_s the position of the electron sheet, which can be at various heights between the gap b; h_s is the Euclidean distance between a sheet segment and the point normal to electron position; $k_e = 8.8976 \text{ x } 10^9 Nm^2C^{-2}$ (Coulomb constant); w_s is the width of the space charge sheet, which for convenience is assumed to be a (the width of the gap) and l_s is the length stretched by the space charge sheet (see *Fig*. 3). To compute and analyze the electron trajectory, the 4th-Order Runge-Kutta method was used to solve equation (9).

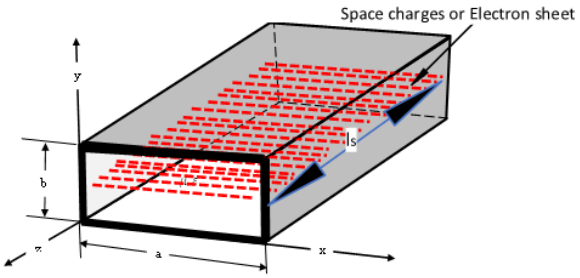

Fig. 2 Illustration of space charge sheet formed between metal surfaces of a rectangular waveguide component

After each collision, the distribution average for true secondary electrons was computed using a combination of Vaughan empirical formulation and Poisson distribution while the probability distribution for elastic and inelastic reflected electrons was computed using models provided by [11].

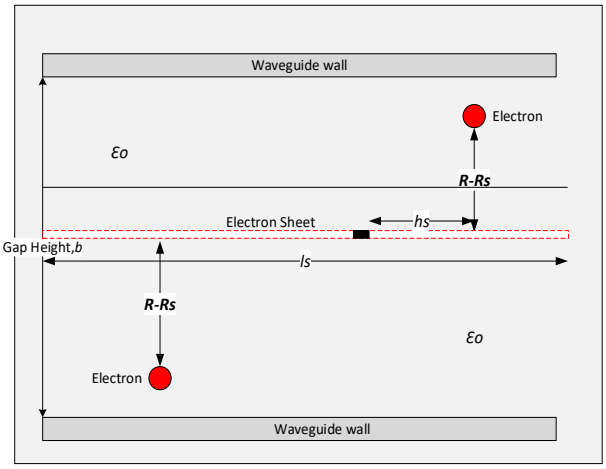

Fig. 3 Illustration of space charge sheet parameters

The energy distribution for the true secondary electrons was calculated as follows: for each emitted electron,

i. The first of the n secondaries is assigned the maximum possible energy, i.e.,

$$E_{s,max} = \frac{wkfn}{3} \quad (12)$$

ii. and for the subsequent ones,

$$E_s(next) = E_s(previous) - E_s(previous) \times random\ value \quad (13)$$

The *random value* is generated using a Gaussian probability distribution [2], [12-14]. Parameter E_s is the emission energy of the secondary electron and $wkfn$ is the work function of the coating material. The elastically reflected electron retains the same energy as that of the primary electron that generated it. Thus,

$$E_s = E_p \quad (14)$$

An inelastic collision result in a transfer (loss) of a percentage of the impacting electron energy to the impacted atom. Because the atom is massive with respect to the electron, it barely recoils and the electron reflects with a velocity nearly equal in magnitude to its incident velocity. The transferred energy is a function of the ratio of the masses of the electron, m_e, and impacted atom, m_{atom}, and the velocity of the impact electron, v_e [15], [16]. This is given as,

$$E_{transferred}(eV) = \left(4 * \left(\frac{m_e}{m_{atom}}\right) * \frac{1}{2} m_e {v_e}^2\right)/q \quad (15)$$

Hence, on reflection the energy of the electron is computed as

$$E_s = E_{impact} - E_{transferred} \quad (16)$$

International Journal of Engineering Applied Sciences and Technology, 2020
Vol. 5, Issue 3, ISSN No. 2455-2143, Pages 20-25
Published Online July 2020 in IJEAST (http://www.ijeast.com)

III. ALGORITHM IMPLEMENTATION

The algorithm was implemented with Matlab. The code adopted a multiple electron releasing (MER) scheme approach. In this case, an initial minimum one thousand virtual primary electrons are released from the bottom plate of the waveguide (a reduced height WR1800 0.433m x 0.102m silver-coated rectangular waveguide). These electrons are tracked individually and simultaneously for 20-gap crossings [17], [18]. The influence of the electric field E, magnetic field B and field due to space charges E_{sc} were accounted for. The waveguide walls are coated with silver coating and reflected electrons (elastic and inelastic reflected electrons) were also accounted for. Simulations were run for $\sigma_s \gg \sigma_{eT}$, $\sigma_s = \sigma_{eT}$, $\sigma_s \ll \sigma_{eT}$ and $\sigma_s = 0$; σ_{eT} is the total charge density of the emitted electrons.

IV. RESULTS AND DISCUSSION

The validation of the algorithm was discussed extensively in [3], [4]. For the current work, four (4) scenarios were implemented: $\sigma_s \gg \sigma_{eT}$, where $\sigma_s = 50 * \sigma_{eT}$; $\sigma_s = \sigma_{eT}$; $\sigma_s \ll \sigma_{eT}$ where $\sigma_s = 1/50 * \sigma_{eT}$; and $\sigma_s = 0$, all at 230 kW 500 MHz operating frequency. Multiple run cycles per scenario was done to ensure that electron emissions points would cover as many random possible positions from the waveguide plate. The space charge sheet was held in stationary state between the gap crossing, exerting field influence on emitted electrons as they cross to-and-fro the gap. The results of each simulation are shown in *Figs*. 4-7. MP is initiated when $\delta \geq 1$.

Fig. 4 is the plot of secondary electron yield vs. the number of gap crossings (δ *vs. N*) for $\sigma_s \gg \sigma_{eT}$. δ consists of four secondary electron yield components, $\delta_1, \delta_2, \delta_3$ *and* δ_4, which resulted from four independent simulation runs. There is an initial decrease in δ output. However, it begins to increase by the 4th crossing until all four δ components cross the MP initiation threshold, i.e., $\delta = 1$, at the 8th gap grossing. This increase in δ continues until the 10th gap crossing when there is a sharp drop. Increment restarts again at the end of the 11th crossing. The observed decrement in δ values especially after the 10th crossing may be attributed to mutual electron-electron repulsions.

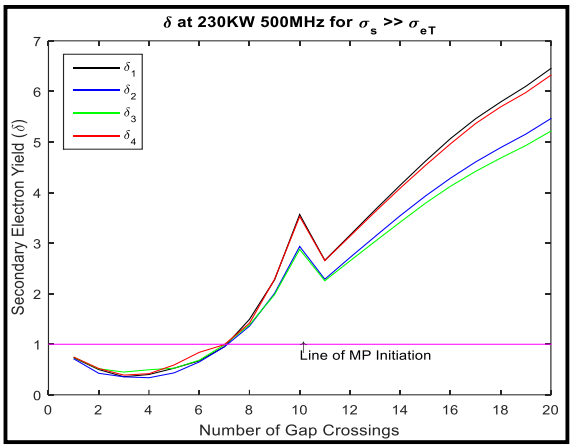

Fig. 4: Plot of δ vs. N for $\sigma_s \gg \sigma_{eT}$

Fig. 5 is the plot of δ *vs. N* for $\sigma_s = \sigma_{eT}$. Generally, the plot shares similar features with *Fig.* 4. However, unlike *Fig.* 4, δ_4 crosses the MP initiation threshold at the 7th gap grossing; δ_1, δ_2, and δ_3 cross at the 8th crossing.

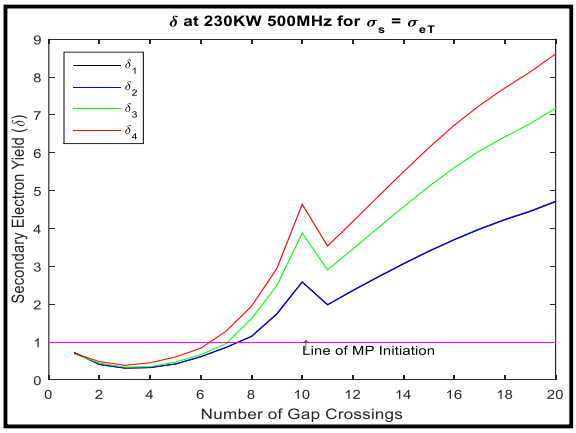

Fig. 5: Plot of δ vs. N for $\sigma_s = \sigma_{eT}$

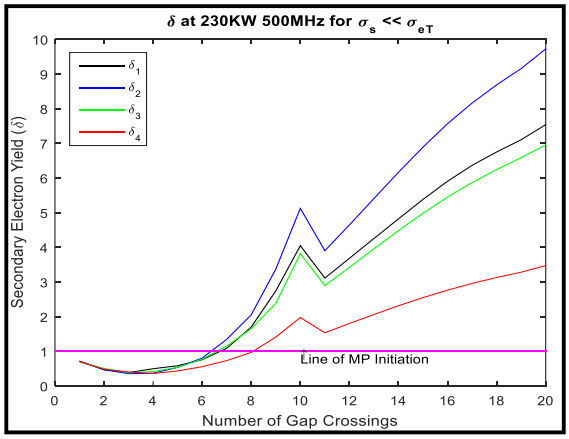

Fig. 6: Plot of δ vs. N for $\sigma_s \ll \sigma_{eT}$

International Journal of Engineering Applied Sciences and Technology, 2020
Vol. 5, Issue 3, ISSN No. 2455-2143, Pages 20-25
Published Online July 2020 in IJEAST (http://www.ijeast.com)

Fig. 6 is the plot of δ *vs. N* for $\sigma_s \ll \sigma_{eT}$. The plot shares similar output features with *Figs.* 4 and 5. It was observed that δ_1, δ_2 and δ_3 cross the MP initiation threshold at the 7th gap crossing; δ_4 crosses at the 8th crossing.

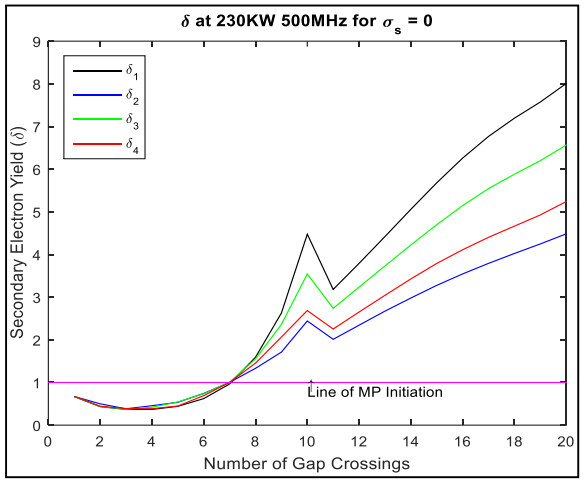

Fig. 7: Plot of δ vs. *N* for $\sigma_s = 0$

Fig. 7 is the plot of δ *vs. N* for $\sigma_s = 0$. Condition $\sigma_s = 0$ means that the effect of the electron sheet is assumed negligible. It was observed that all four δ components cross the MP initiation threshold by the 7th gap crossing.

Following the examination of the results, the preceding observations can be summarized thus:

i. For all simulation scenarios, at the start of each iteration, there seemed to be a decrement in electron population size. This may be due to the mutual electron-electron repulsion brought in by space charge forces causing a phase error, which impairs the phase-focusing mechanism [19], and makes the electron number decrease. However, as the electrons continued to cross the gap and impact the component surface, a continual increase in electron population size is observed.

ii. In all scenario runs, multipactor initiation is observed and is unaffected by the presence or absence of space charges. A comparison of results in which space charge field effect was considered with results where they were not considered did not show significant difference as multipactor showed signs of initiation by the 7th or 8th gap crossing but confirmed by the 10th crossing. This may be as a result of phase-focusing effect [19] or the high impact energies of the multipacting electrons [20].

iii. The lesser the quantity of space charges, the earlier the secondary electron yields cross the MP initiation threshold. This suggests that, despite the fact that the presence of space charges do not necessary hinder the initiation of multipaction (as stated in ii above), there presence however, retards the rate at which secondary electrons are emitted.

V. CONCLUSION

This work investigated the effect of space charges on the initiation of multipactor in TE_{10} mode rectangular waveguide structures, using a developed reflected-electron-inclusive MP prediction algorithm. Space charges are known to introduce electron-electron repulsion forces which in this case can alter significantly the trajectory of possible multipactor-initiating electrons. Obtained results suggested that the presence of these space charges in the waveguide could impair the phase-focusing mechanism of the transiting electrons thus retarding the rate at which secondary electrons are emitted from the waveguide surface. This was inferred from the fact that the lesser the population size of space charges, the larger the number of electron emissions and thus the earlier the secondary electron yields crossed the MP initiation threshold. Eventually however, the presence of space charges, irrespective of population size, is not able to hinder the initiation of multipaction especially when high-energy electron impacts are involved. The high-energy electrons are able to restore and sustain the phase-focus mechanism.

VI. REFERENCES

[1] Arregui I., Anza S., Teberio F., Vicente C., Arnedo I., *et al.* (2011). High-Power Alternative to the Design of Spurious-Free Classical E-plane Corrugated Filters, presented at the Proc. of Int'l Workshop on Multipactor, Corona and Intermodulation (MULCOPIM), Valencia, Spain, Session 2.

[2] Vicente C., Mattes M., Wolk D., Hartnagel H., Mosig J. and Raboso D. (2005). FEST3D - A Simulation Tool for Multipactor Prediction, in Proc. of 5th Int'l Workshop on Multipactor, Corona and Intermodulation (MULCOPIM), ESTEC-ESA, Noordwijk, The Netherlands, (pp. 11-17).

[3] Akoma H.E.C.A., and Adediran Y.A. (2012). Influence of Reflected Electrons on Multipactor Prediction for Rectangular Waveguides", Cyber Journals: Multidisciplinary Journals in Science and Technology, Journal of Selected Areas in Telecommunications (JSAT), (pp. 17-22).

[4] Akoma H.E.C.A., and Adediran Y.A. (2012). Investigating the Role of Reflected Electrons in Multipactor Breakdown for TE_{10} Mode Configured Rectangular Waveguides", International Journal of

Advances in Engineering & Technology, ©IJAET ISSN: 2231-1963, Vol. 4, Issue 2, (pp. 1-10).

[5] Li Y., Wang X., and Cui W. (2011). Space Charge Effects on Multipactor Discharge of Microwave Components, in Proc. 4th IEEE International Symposium on Microwave, Antenna, Propagation and EMC Technologies for Wireless Communications, doi:10.1109/MAPE.2011.6156311, 978-1-4244-8268-9/1, Nov. 2011, (pp. 481-484).

[6] Anza S., Vicente C., Raboso D., Gil J., Gimeno B. and Boria V.E. (2008). Enhanced Prediction of Multipaction Breakdown in Passive Waveguide Components including Space Charge Effects, 2008 IEEE MTT-S International Microwave Symposium Digest, Atlanta, GA, USA, doi:10.1109/MWSYM.2008.4633247, (pp. 1095-1098).

[7] Nieter C., Roark C.M., Stoltz P.H. and Tian K. (2009). Benchmarking Multipacting Simulations in Vorpal, in Proc. of 23rd Particle Accelerator Conference (PAC09), Vancouver, BC, Canada, (pp. 1-3).

[8] Somersalo E., Yl¨a-Oijala P. and Proch D. (1998). Computational Methods for Analyzing Electron Multipacting in RF Structure, Particle Accelerators, Vol. 59, (pp. 107-141).

[9] Coves A., Torregrosa-Penalva G., Vicente C., Gimeno B. and Boria E. (2008). Multipactor Discharges in Parallel-Plate Dielectric-Loaded Waveguides Including Space-Charge Effects, IEEE Transactions On Electron Devices, Vol. 55, No. 9, (pp. 2505-2511).

[10] Serway R.A., and Jewett J.W.J. (2010). Physics for Scientists and Engineers with Modern Physics, 8th Ed., Brooks/Cole Pub., (pp. 667-675).

[11] Juan L, Francisco P., Manuel A., Luis G., Isabel M., Elisa R. and David R.G. (2006). Multipactor Prediction for On-Board Spacecraft RF Equipment with the MEST Software Tool, IEEE Transactions on Plasma Science, Vol. 34, No. 2., (pp. 476-484).

[12] Becerra G.E. (2007). Studies of Coaxial Multipactor in the Presence of a Magnetic Field, M.Sc. thesis, Department of Nuclear Science and Engineering, Massachusetts Institute of Technology.

[13] Furman M.A., and Pivi M.T.F. (2003). Simulation of Secondary Electron Emission Based on a Phenomenological Probabilistic Model, Center for Beam Physics, Accelerator and Fusion Research Division, CA, USA, Report No: LBNL-52807, SLAC-PUB-9912, doi: 10.2172/835149

[14] Seviour R. (2005). The Role of Elastic and Inelastic Electron Reflection in Multipactor Discharges, IEEE Transactions on Electron Devices, Vol. 52, No. 8, (pp. 1927-1930).

[15] Landau L.D., and Lifshitz E.M. (2006). Mechanics: Course of Theoretical physics, 3rd Ed., Vol. 1, Butterworth and Heinemann Publication, (pp. 41-53)

[16] Bellan P.M. (2013). Fundamentals of Plasma Physics, 1st Ed., Cambridge University Press, (pp. 14-16).

[17] Space Engineering, Multipcation Design and Test (2013). ECSS-E-20-01A Rev.1 1

[18] Yla-Oijala P. (1999). Multipacting Analysis and Electromagnetic Field Computation by the Boundary Integral Equation Method in RF Cavities and Waveguides; Ph.D. Dissertation, Division of Mathematical Theory and Applications of Electromagnetic Fields, Rolf Nevanlinna, Institute Faculty of Science University of Helsinki.

[19] Vaughan J.R.M. (1988). Multipactor, IEEE Transactions on Electron Devices, Vol. 35, No. 7, (pp. 1172 – 1180).

[20] Kishek R. A., and Lau Y. Y. (1996). A novel phase focusing mechanism in multipactor discharge, Phys. Plasmas, American Institute of Physics, Vol. 3 (5), (pp. 1481-1483).